Blucher Mechanical Engineering Proceedings
May 2014, vol. 1 , num. 1
www.proceedings.blucher.com.br/evento/10wccm

10th World Congress on Computational Mechanics
8-13 July 2012 • São Paulo • Brazil

MULTI PHYSICS SIMULATION OF LIQUID DROPLET IMPINGEMENT EROSION

K. Fujita[1] , M. Suzuki[2] and M. Yamamoto[3]

[1]Graduate school of Mechanical Engineering, Tokyo University of Science

[2]Clean Engine Team, Aviation Program Group, Japan Aerospace Exploration Agency

[3]Department of Mechanical Engineering, Tokyo University of Science
(yamamoto@rs.kagu.tus.ac.jp)

Abstract. *Pipe wall thinning is one of the most serious problems in a power plant operation. The analysis of pipe wall thinning phenomenon is a critical issue for the safety and to increase the operation rate of power plants. One of the main causes of pipe wall thinning phenomenon of power generation facilities is the liquid droplet impingement erosion (LDIE). It is well known that the LDIE progress is classified into three stages; incubation, acceleration and steady-state. Conventionally, the steady-state stage has been investigated. In this study, we develop a numerical procedure to predict the incubation period and the steady-state stage. Additionally, we simulate the LDIE using computational fluid dynamics. The simulation results are compared with the experiment. As the results, it is shown that the simulation results are in qualitative agreement with the experimental data. And thus we confirm that the numerical procedure of LDIE model proposed in this study is fairly validated.*

Keywords: *Droplet Erosion, Gas-Liquid Two-Phase Flow, Computational Fluid Dynamics*

1. INTRODUCTION

Pipe wall thinning is one of the most serious problems in a power plant operation. Pipe wall thinning is the phenomenon in which inner wall of a pipe is thinning due to corrosion or erosion by fluid flowing. Until today, many pipe rupture accidents have been reported and most of them are caused by pipe wall thinning.

One of the main cause of pipe wall thinning phenomenon of power generation facilities is the liquid droplet impingement erosion (LDIE). LDIE is the phenomenon that the material is damaged by the impact pressure when liquid droplets impinge on the material surface. Since LDIE locally occurs, it is difficult to detect the damaged area. Furthermore, since there are many pipes in a plant and the operating conditions are various, LDIE can occur under different situations. This fact has a significant influence on the regular inspection process and

leads to the reduction of operation rate [1]. Furthermore, it is difficult and extreamly expensive to make the experimental equipments for LDIE under various conditions. Therefore, the LDIE simulation model that can reproduce any LDIE phenomena is strongly required.

It is well known that the LDIE progress is classified into three stages; incubation, acceleration and steady-state. In the incubation stage, plastic deformation takes place on the material surface without mass loss. After this initiation stage, the mass loss commences and proceeds at an increasing rate with time. This is termed as acceleration stage. The mass loss rate accelerates to a terminal value, referred to maximum rate stage. In the maximum rate stage, the erosion rate remains constant for a certain period, thus the maximum rate stage is also known as steady-state stage. Most of the material life is consumed in the steady-state stage. Generally, the researches on LDIE have focused on only the steady-state. However, when an incubation stage is not considered, it is obvious that erosion damage cannot be appropriately estimated.

Therefore, the purpose of this study is to develop and validate the numerical procedure of LDIE simulation model including an incubation stage and a steady-state stage using computational fluid dynamics. As a result, it is confirmed that the present LDIE model can qualitatively predict the damage of LDIE under the different conditions of the material hardness and the droplet.

2. NUMERICAL PROCEDURE

Flow chart of the present LDIE simulation is shown in Figure 1. The prediction of the LDIE phenomenon is composed of three steps which are flow computation, droplet tracking and erosion estimation. Additionally, Euler-Lagrange coupling is used for solving the gas-liquid two-phase flow.

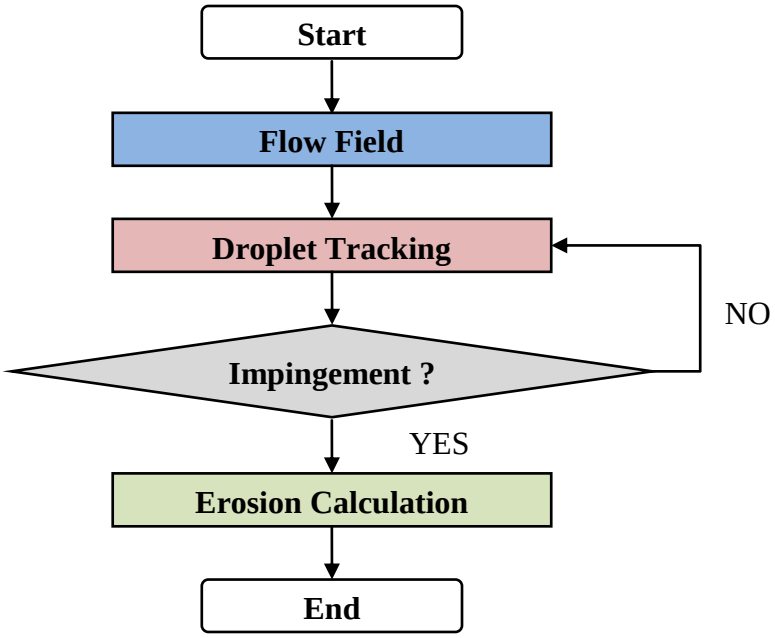

Figure 1 Flow chart of present LDIE simulation

2.1. Flow field

In this study, the flow field is assumed to be an axisymmetric, compressible and turbulent. The governing equations are Favre-averaged continuity, Navier-Stokes and energy equations. The standard k-ε turbulence model (Launder and Spalding, [2]) is applied to estimate turbulence. Since the standard k-ε model excessively predict turbulence energy production for irrotational strain, Kato-Launder's modification (Kato and Launder, [3]) is adopted. The governing equations are discretized using second-order upwind TVD scheme (Yee and Harten, [4]) for the inviscid terms, second-order central difference scheme for the viscous ones, and 4-stage Runge-Kutta method for the time integration.

2.2. Droplet tracking

Droplet tracking computation is based on a Lagrangian approach. The computation uses the following assumptions:

- The droplet is solid and spherical.
- The droplet does not break up.
- The droplets do not interact with each other.
- The droplets do not affect on the flow field (one-way coupling).
- The initial droplet velocity is equal to the gas velocity at the release point.

The equation of droplet motion is given by

$$\frac{d\vec{U}_p}{dt} = \frac{3}{4} C_D \frac{\rho_f}{\rho_p} \frac{1}{d_p} \vec{U}_r \left| \vec{U}_r \right| \tag{1}$$

where t is the time, U_p is the droplet velocity, U_r is the relative velocity between the gas and the droplet, d_p is the droplet diameter, and ρ_f and ρ_p are the gas and the droplet density respectively. The drag coefficient C_D is expressed as:

$$C_D = \frac{24}{\mathrm{Re}_p} \left(1 + 0.15 \mathrm{Re}_p^{\,0.687} \right) \tag{2}$$

where Re_p is the Reynolds number of the droplet based on the diameter and the relative velocity between the gas and the droplet.

2.1. Erosion calculation

Miyata and Isomoto [5] experimentally found that eroded mass is proportional to the square of droplet impinging velocity. Therefore, the equation of eroded mass of materials is represented as

$$E = Cu^2, \quad C = \alpha Hv^{\beta} \tag{3}$$

where E [m^3/kg] is the eroded mass to the unit mass of droplets and u[m/s] is the impingement velocity of a droplet. C is the coefficient that depends on the property of material, and it is defined by Vickers hardness Hv [GPa] and empirical constants α and β. α and β are 4.04×10^{-4} and -2.75 respectively.

In an actual erosion, material begins to be eroded after an incubation period. The equation (3) is for a steady-state stage and thus the incubation period is not considered. The Incubation period is described by erosion rate and characteristic depth Dc, as shown in Figure 2. Furthermore, it is known that the characteristic depth Dc depends on the mechanical property of material and the droplet impingement velocity [5]. In this study, the characteristic depth Dc [mm] is approximated by the following equation,

$$Dc = \kappa u^{\lambda} \tag{4}$$

where κ and λ are model coefficients and are determined below.

In Figure 3, the relations between the characteristic depth and the droplet impingement velocity in the experiment are shown. In the present study, we originally propose approximate formula where κ and λ are fitted to the experimental data and they are represented by Vickers hardness Hv to estimate Dc for different materials. κ and λ are respectively defined as following equations.

$$\kappa = -2.01Hv + 10.6 \tag{5}$$

$$\lambda = 0.373Hv^2 - 1.24Hv \tag{6}$$

In the computations, we reproduce the incubation period by setting virtual mass to the wall surface. Multiplying the characteristic depth Dc by the surface area of a cell gives the virtual mass. When the virtual mass is consumed by the LDIE, actual erosion damage is considered on the material surface.

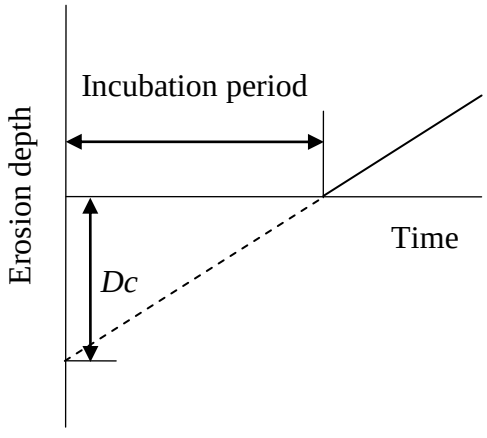

Figure 2 Characteristic depth

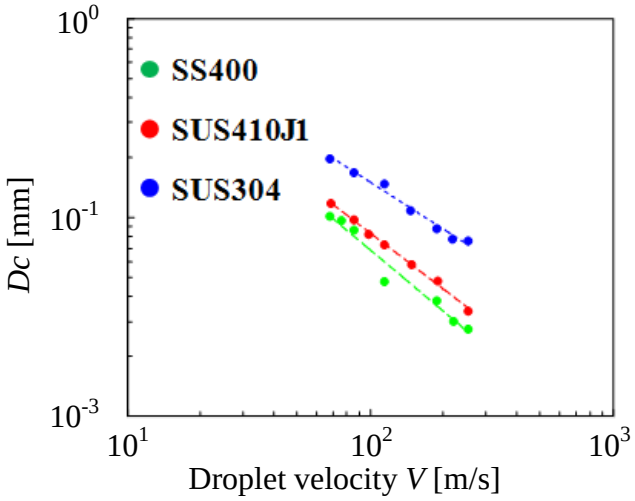

Figure 3 Characteristic depth and droplet velocity

3. COMPUTATIONAL CONDITION

3.1. Computational domain

In this study, the experiment of Miyata and Isomoto [5] is compared with the calculation results to validate the present LDIE model. In Figure 4, the schematic view of test section and computational domain are exhibited. Water jet test is the method for estimating the damage of specimen due to LDIE by spraying high velocity water against the specimen. In this experiment, when the distance between nozzle and specimen (Stand off Distance, SOD) is over about 150 mm, water column actively begins to break up and make droplets. Additionally, when SOD is about 200 mm, the erosion damage is the greatest. Therefore, the flow computational domain is the area where the distance from the nozzle exit is 150~200 mm and the total computational domain is the area that the specimen of 5 mm thickness is added to the flow computational domain (i.e. red region in Figure 4). The total number of the grid points is 20,300, that for the flow field is 101 × 161 and for the inside of the specimen is 101 × 40.

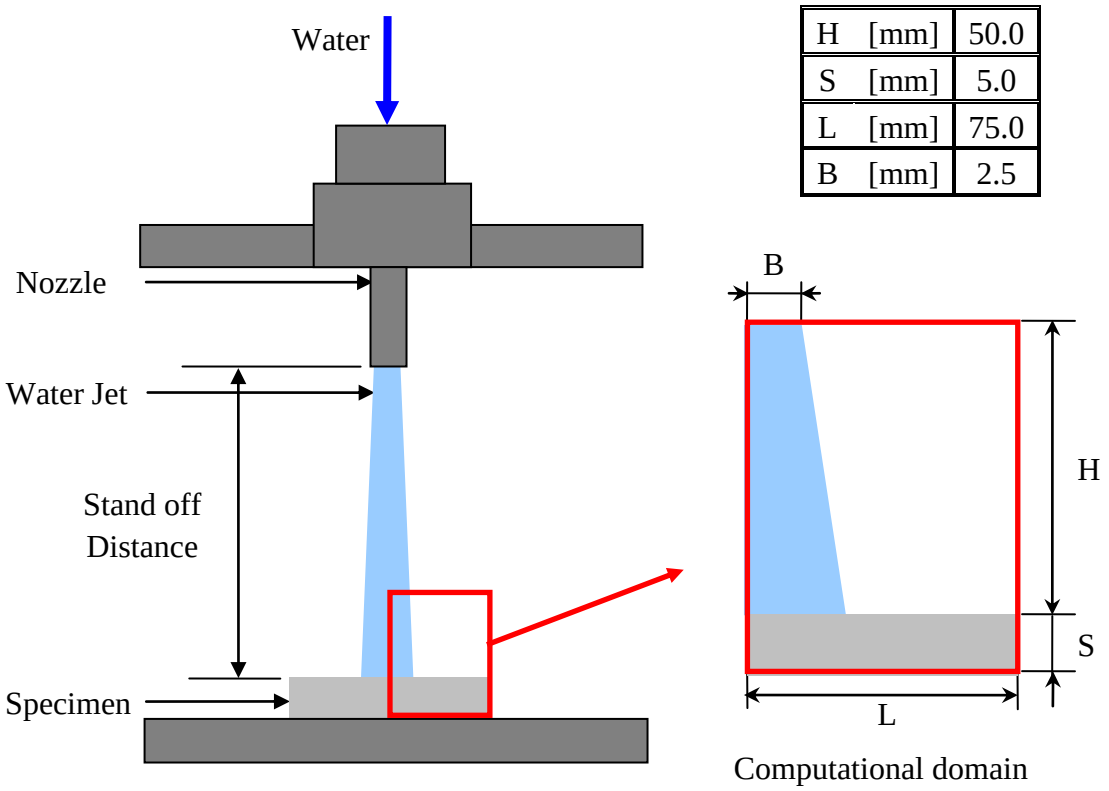

H	[mm]	50.0
S	[mm]	5.0
L	[mm]	75.0
B	[mm]	2.5

Figure 4 Schematic view of test section and computational domain

3.2. Operating condition

The working fluid is air and the inlet velocity is fixed by the injection pressures (30~90MPa). The static temperature of 293.15 K and the turbulent quantities are fixed at the

inlet boundary, and the static pressure of 101.3 kPa is fixed at the outlet boundary. It is assumed that the droplets have a single droplet diameter, and the droplets are uniformly distributed over the inlet boundary. The tracked droplet number is 10^5 so that the total weight of the tracked droplets is matched with the experiment. General carbon steel SS400, martensite stainless steel SUS410J1 and austenite stainless steel SUS304 are used for the specimens. The inlet velocity V and the droplet diameter D depending on the injection pressures P are listed in Table 1. Furthermore, Vickers hardness Hv and the density ρ are summarized for each material in Table 2.

Table 1 Computational conditions

P	[MPa]	30	50	70	90
V	[m/s]	152	194	229	258
D	[mm]	0.07	0.06	0.05	0.04

Table 2 Material properties

		SS400	SUS410J1	SUS304
Hv	[GPa]	1.46	2.20	2.50
ρ	[kg/m^3]	7.80×10^3	7.75×10^3	7.93×10^3

4. NUMERICAL RESULTS AND DISCUSSION

4.1. Flow field

The distributions of Mach number and turbulent kinetic energy in the 30 MPa injection pressure case are respectively illustrated in Figure 5 and Figure 6. As Figure 5 indicates, the air vertically flows to the material until just before impingement. Moreover, it is observed that the Mach number is nearly 0 at the wall vicinity. Therefore, the formation of a stagnation point is confirmed in the center of impinging flow. Then, the air flows along the wall surface from the stagnation point to the both sides.

As shown in Figure 6, the turbulent kinetic energy is higher at the sides of the jet flow before impingement and the wall vicinity of sides of the stagnation point. For this reason, the former is considered because strong shear layer is formed between the air and the high velocity jet flow, and the latter is due to the air accelerate along the wall surface after impingement.

As stated above, the validity of this flow computation about reproduction of the jet flow is qualitatively confirmed. Note that a similar tendency can be seen in other injection pressure cases. Therefore, we decided that the computed flow fields are used for calculating droplet trajectories.

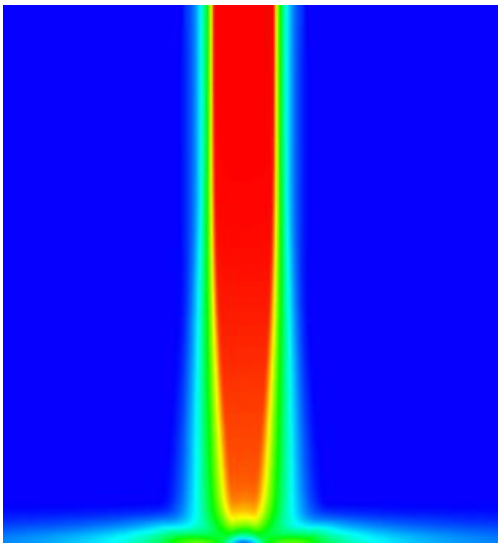

Figure 5 Mach number distribution

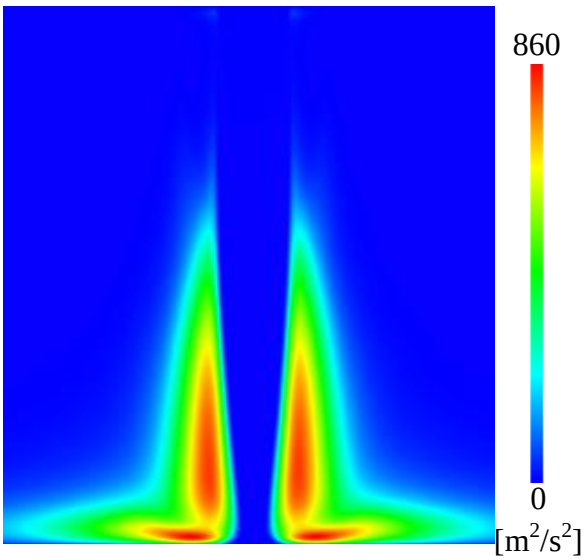

Figure 6 Turbulent kinetic energy distribution

4.2. Erosion calculation

The eroded wall shape of SUS304 at 418 s is shown in Figure 7. The abscissa x is the distance from the center. In any cases, the eroded width is about 5 mm and is in agreement with the droplet inflow width. Therefore, the diffusion of droplets is small. For this reason, it is considered that the droplet is insignificantly affected by the change of gas flow since the mass of liquid is much larger than that of gas and the inertia force is dominant. Furthermore, the erosion depth is almost uniform and the width is nearly same as the inlet width. In this study, the average of the erosion depth in the half area of the erosion width ED_{ave} is compared with the experimental results.

The time history of ED_{ave} and the experimental results for each case are shown in Figure 8. The characteristic depth Dc and the incubation period of the experiment and the computation are summarized in Table 3 and Table 4. The incubation period is the point at the intersection of horizontal axis with the approximate line for the experimental and computational results.

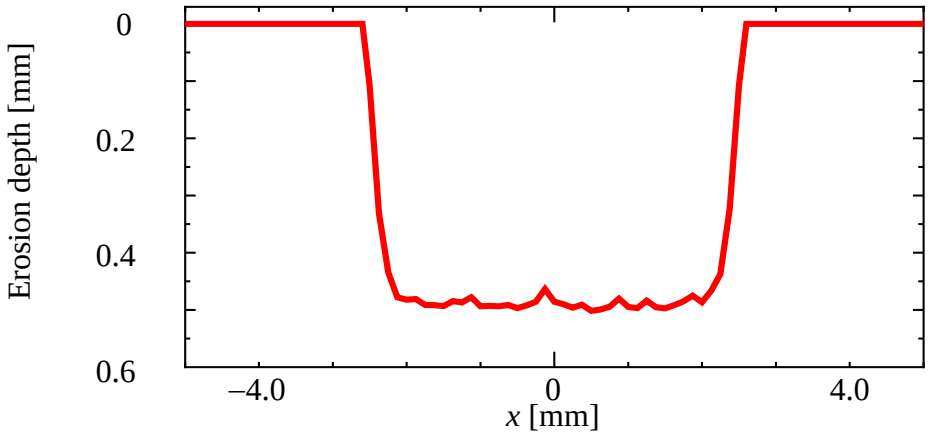

Figure 4 Eroded surface

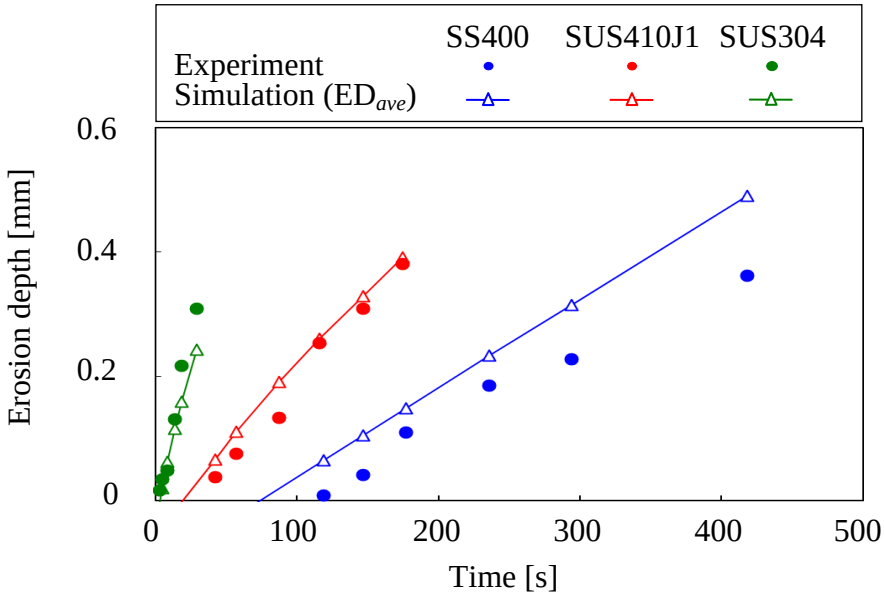

(a) Effect of materials (30 MPa)

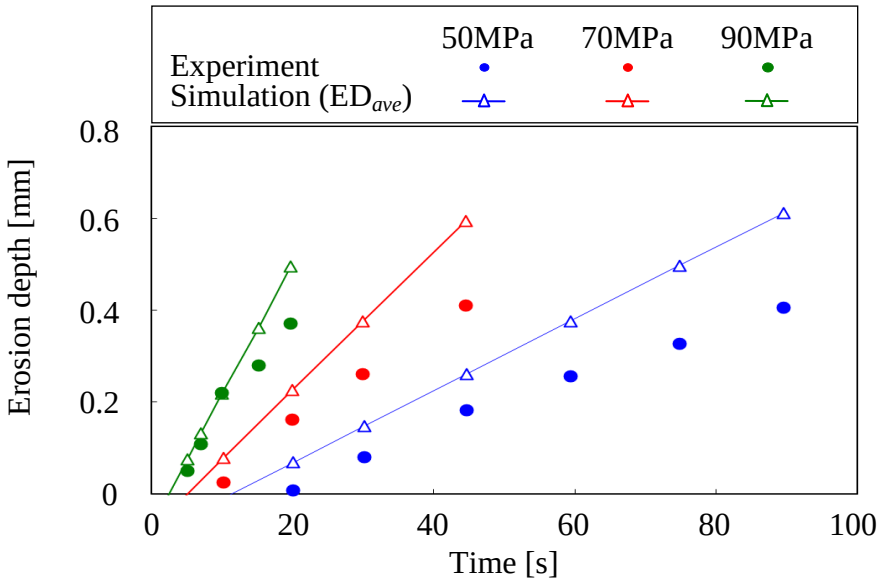

(b) Effect of water pressure (SUS304)

Figure 8 Time history of erosion depth for different material and water pressure

The time history of erosion depth for each material at the 30MPa injection pressure case is shown in Figure 8 (a), and the characteristic depth *Dc* and the incubation period in those cases are listed in Table 3. The general carbon steel SS400, the martensite stainless steel SUS410J1 and the austenite stainless steel SUS304 have lager Vickers hardness in this order. As shown in Figure 8 (a), in both the experiment and the computation, the larger Vickers hardness of the material is, the lower erosion rate becomes. Additionally, since the difference of Vickers hardness between SUS410J1 and SUS304 is not so much in comparison with SS400, the difference of erosion rates is small. However, as indicated in Table 3, since these materials have different incubation periods, the difference of the erosion depth is large. Comparing the experiment and the computation, the similar tendency can be observed. Therefore,

Table 3 Characteristic depth *Dc* and incubation period (30 MPa)

	Characteristic depth *Dc*			Incubation period		
	Exp. [mm]	Sim. [mm]	Err. [%]	Exp. [s]	Sim. [s]	Err. [%]
SS400	0.0302	0.0447	48	3.41	3.91	14.7
SUS410	0.0530	0.0561	5.8	22.8	18.4	19.3
SUS304	0.119	0.109	8.7	101	72.6	28.1

Table 4 Characteristic depth *Dc* and incubation period (SUS304)

	Characteristic depth *Dc*			Incubation period		
	Exp. [mm]	Sim. [mm]	Err. [%]	Exp. [s]	Sim. [s]	Err. [%]
50 MPa	0.0903	0.0898	0.55	16.2	11.2	30.9
70 MPa	0.0792	0.0791	0.16	7.17	5.15	28.2
90 MPa	0.0718	0.0722	0.43	2.36	2.46	4.24

it is clear that this LDIE model can describe the difference of the erosion rates and the incubation periods for different materials.

The time history of the erosion depth for SUS304 in each injection pressure (50~90MPa) case is shown in Figure 8 (b). The characteristic depth *Dc* and the incubation period in those cases are listed in Table 4. Clearly, the lager the injection pressure is, the smaller the droplet diameter becomes. However, following the knowledge of the previous study, it is assumed that the droplet diameter has less effect on droplet tracking and erosion mass, the effect of impingement velocity is only noted here. As shown in Figure 8 (b), in both the experiment and the computation, the lager injection pressure is, the faster erosion rate is. Incubation period is shorter when injection pressure is larger. A similar characteristic can be observed in the experiment.

Although the tendency of the computation agrees well with the tendency of the experiment, as regards in erosion rate, the harder material is, the greater error becomes. The effect of liquid film at the eroded area is considered as the main factor in this error. In this study, it is assumed that the droplets impinging on the specimen immediately disappear, in other words the droplets have not been tracked after impingement. However, in the experiment, the water does not disappear but exists in the eroded cavity, and liquid film is formed there. The liquid film may cushion the shock of droplet impingement, which leads to a certain decrease of erosion rate. Since the present LDIE model does not take into account the existence of the liquid film in the eroded cavity, the mismatch for the experiment might be observed. In order to clarify this point, we will need further investigations.

5. CONCLUSION

We developed the numerical procedure of liquid droplet impingement erosion including the incubation period and the steady-state stage. The knowledge obtained in the present study is summarized below:

- The present LDIE model can qualitatively predict the damage of LDIE under the different conditions of the material hardness and the droplet.
- The incubation period can be modeled by the characteristic depth *Dc*.
- The effect of liquid film in the eroded cavity is considered as one of error factors.

6. REFERENCE

[1] Harold, M.C. and Jeffrey, S.H., "Erosion in nuclear piping systems", *Journal of Pressure Vessel Technology.*, 1-11, 2005.

[2] Launder, B.E., Spalding, D. B., "The Numerical Computation of Turbulent Flows", *Computer methods in applied mechanics and engineering Vol.3 No.2*, 269-289, 1974.

[3] Yee, H. C., "Upwind and Symmetric Shock-capturing Schemes", *NASA-TM-89464*, 1987.

[4] Kato, M., Launder, B. E., "The Modeling of Turbulent Flow Around Stationary and Vibrating Square Cylinders", *Proceedings of 9th Symposium on Turbulent Shear Flows*, 10.4.1-10.4.6, 1993.

[5] Miyata, H. and Isomoto, Y., "Erosion Phenomenon caused by Water Droplet Impingement and Life Prediction of Industrial Materials", *Zairyo-to-Kankyo.* 57, 1-24, 2008.